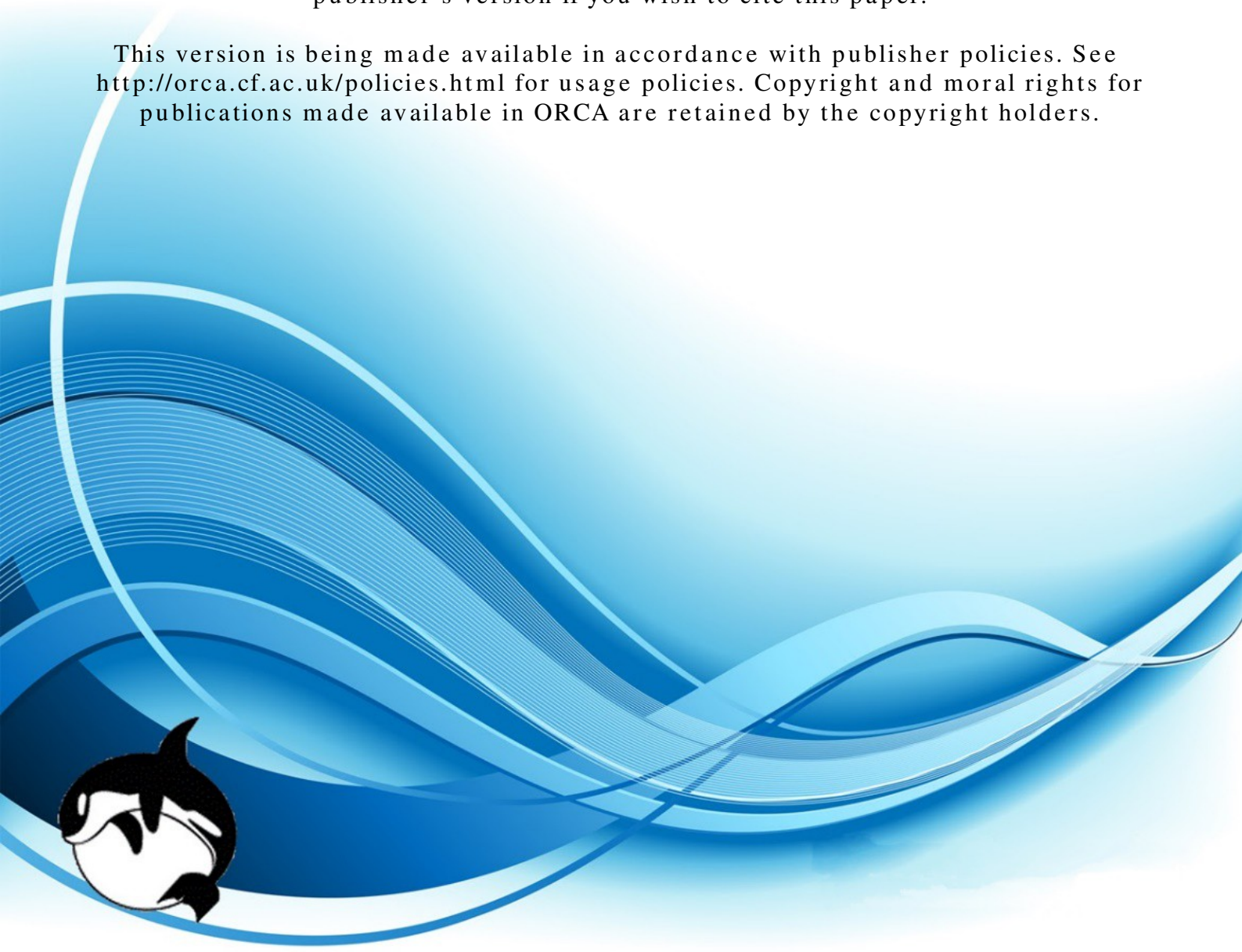

A 3D coupled finite element model for simulating mechanical regain in self-healing cementitious materials

Brubeck Lee Freeman, Anthony Jefferson

*freemanbl@cardiff.ac.uk, Cardiff University School of Engineering, The Parade, Cardiff, CF24 3AA, UK

jeffersonad@cardiff.ac.uk, Cardiff University School of Engineering, The Parade, Cardiff, CF24 3AA, UK

Keywords: Embedded strong discontinuity, Self-healing, Finite element method, Coupled model, Constitutive, Damage-healing mechanics, Flow in discrete cracks, Cohesive zone model

Abstract

This study presents a new 3D coupled model for simulating self-healing cementitious materials. The mechanical behaviour is described using a damage-healing cohesive zone model that is implemented using a new embedded strong discontinuity hexahedral element. The transport component of the model considers the flow of healing agent through discrete cracks, governed by the mass balance equation with Darcy's law being employed for the healing agent flux. The dependency of the mechanical response on the healing agent transport is accounted for through a local crack filling function that represents the amount of healing agent available to undergo healing. The healing itself is described by a generalised healing front model that simulates the accumulation of healed material within the crack, emanating from the crack faces. The performance of the model is demonstrated through the consideration of a healing front study and experimental tests on self-healing cementitious specimens. The examples consider a vascular self-healing cementitious specimen that uses a sodium silicate solution as the healing agent and the autogenous healing of a cementitious specimen with and without crystalline admixtures. The results of the validations show that the model is able to reproduce the experimentally observed behaviour with good accuracy.

1. Introduction

The performance of infrastructure materials is greatly hindered by the presence of cracks. This reduction in performance affects both the mechanical behaviour in terms of stiffness and strength, and the durability, as cracks act as pathways for moisture and aggressive ions. Whilst the formation of cracks in cementitious materials is all but inevitable, a great deal of progress has been made on the development of self-healing systems that heal cracks as they form (De Belie *et al.*, 2018). Alongside this, significant progress has been made on the development of numerical models for simulating the self-healing behaviour (Jefferson *et al.*, 2018). Many of the models developed have focussed on mechanical damage-healing behaviour (Voyiadjis, Shojaei and Li, 2011; Zhang and Zhuang, 2018; Esgandani and El-Zein, 2020), though there have been a number that considered the associated transport processes (Aliko-Benítez, Doblaré and Sanz-Herrera, 2015; Chitez and Jefferson, 2016; Gilabert *et al.*, 2017). In addition to this, there is an ever increasing number of models being developed that consider the coupled physical processes governing the self-healing response (Hilloulin *et al.*, 2016; Di Luzio, Ferrara and Krelani, 2018; Rodríguez *et al.*, 2019; Cibelli *et al.*, 2022; Jefferson and Freeman, 2022).

The representation of damage in self-healing models has varied, with many of the earlier studies employing a continuum damage mechanics framework (CDM) (Lemaitre and Desmorat, 2005). In such models, damage is represented using one or more damage variables that express the relative area of micro-cracked material. The extension of the framework to include healing (termed continuum

damage healing mechanics, CDHM) is achieved through the introduction of one or more healing variables that act as a multiplier on the damaged portion of material (Barbero, Greco and Lonetti, 2005; Voyiadjis, Shojaei and Li, 2011). CDHM models are particularly convenient for simulating healing due to their direct representation of the area available for healing through the damage variable(s). In addition, CDHM theories can be applied in micromechanical models that can naturally account for anisotropic damage and healing (Davies and Jefferson, 2017; Han *et al.*, 2021). Whilst CDHM models provide a convenient framework for predicting self-healing behaviour, the simulation of a number of self-healing systems, including vascular networks (De Nardi, Gardner and Jefferson, 2020), requires a discrete representation of the macro-cracks. To this end, a number of approaches have been employed, including the discrete element method (Zhou *et al.*, 2017), lattice models (Rodríguez *et al.*, 2019), elements with embedded strong discontinuities (Zhang and Zhuang, 2018; Freeman *et al.*, 2020), the extended finite element method (Gilabert, Garoz and Paepegem, 2017) and the lattice discrete particle model (Cibelli *et al.*, 2022).

For representing the healing itself, and the associated mechanical regain, approaches have varied from healing functions derived from thermodynamic potentials (Barbero, Greco and Lonetti, 2005; Voyiadjis, Shojaei and Li, 2011), to mechanistic models that capture the underlying physical processes (Koenders, 2012; Hilloulin *et al.*, 2016; Xin *et al.*, 2020). Xin et al. (2020) presented a crystal pillar growth model for simulating the healing associated with microbially induced calcite precipitation (MICP). The model considered the nucleation of calcite crystals on the crack face that grow in pillar like structures towards the centre of the crack. The model is based on the assumption that mechanical strength and stiffness regain commences when the pillars first bridge a crack and that healing progresses as a function of the relative bridged area. A number of authors have employed cement hydration models, such as HYMOSTRUC (van Breugel, 1995) and CEMHYD3D (Bentz, 1997), to simulate the healing of cracks due to further hydration (Koenders, 2012; Hilloulin *et al.*, 2016). Hilloulin et al. (2016) used a version of CEMHYD3D (CemPP), combined with the Cast3M finite element code, to simulate mechanical regain due to self-healing. The authors found that the mechanical regain was directly related the filling fraction of healed material at the centre of the crack.

The mechanical regain associated with self-healing is directly related to the amount of healing agent and/or moisture available at the damage site. Whilst a number of authors account for this (Aliko-Benítez, Doblaré and Sanz-Herrera, 2015; Di Luzio, Ferrara and Krelani, 2018; Xin *et al.*, 2020), there have been few coupled models to date that consider the transport of healing agents through discrete cracks (Rodríguez *et al.*, 2019; Cibelli *et al.*, 2022; Jefferson and Freeman, 2022). Romero Rodríguez et al. (2019) presented a lattice model for the simulation of crack sealing in cementitious materials containing super absorbent polymers. The model employed Richard's equation to describe the unsaturated moisture flow, with cracked elements being assigned a higher diffusivity, based on Poiseulle flow within a planar crack. The cracking was simulated using a lattice fracture model with crack widths obtained from experimental data. Cibelli et al. (2022) presented a coupled model that linked a discrete hygro-thermo-chemical model, based on that presented by Di Luzio, Ferrara and Krelani (2018), to the lattice discrete particle model of Cusatis, Pelessone and Mencarelli (2011) for describing the mechanical behaviour. Transport through the discrete cracks was simulated by increasing the local diffusivity of cracked elements, through an empirical function of the crack widths. For the simulation of healing, a linear function of the reaction extent was employed, where the reaction affinity accounted for the effects of local moisture content, crack width, amount of crystalline admixture and temperature, through an Arrhenius type term. The performance of the model was demonstrated through the consideration of autogenous healing of a cementitious specimen loaded in three-point bending (Ferrara, Krelani and Carsana, 2014). The model predictions of the mechanical regain were found to be in good agreement with the experimental results.

The aim of this paper is to present a new 3D coupled finite element model for simulating self-healing cementitious materials. The mechanical behaviour of the material is simulated using a damage-healing cohesive zone model that is implemented in a new embedded strong discontinuity hexahedral element. A particular feature of the model is the coupling between the mechanical regain and the transport of healing agent through the discrete cracks, described here using the mass balance equation combined with Darcy's law for the healing agent flux. The mechanical healing is described using a generalised healing front model, originally derived for the curing of adhesives (Freeman and Jefferson, 2020; Jefferson and Freeman, 2022), which we show can accurately simulate other healing mechanisms that involve precipitation of healed material that evolves from the crack faces.

The layout of the remainder of this paper is as follows:

i. Section 2 presents the theoretical basis for the coupled model.
ii. Section 3 presents the numerical implementation including a description of the new embedded strong discontinuity hexahedral element and a description of the coupling between the transport of healing agent and mechanical regain.
iii. Section 4 presents a series of example problems used to validate the model.
iv. Finally, Section 5 presents some concluding remarks from the study.

2. Theoretical basis

Mechanical model

To describe the damage-healing behaviour we employ a cohesive-zone crack plane model (Jefferson and Freeman, 2022) that is applied to an element with an embedded strong discontinuity, whilst the behaviour of the matrix continuum is described by a linear elastic model.

The stress in the matrix material is given by:

$$\boldsymbol{\sigma} = \mathbf{D} : \left(\boldsymbol{\varepsilon} - \boldsymbol{\varepsilon}_{\mathbf{c}} \right), \qquad \forall \mathbf{x} \in \Omega \tag{1}$$

where $\boldsymbol{\sigma}$ and $\boldsymbol{\varepsilon}$ are the stress and strain tensors respectively, $\mathbf{D}$ is the elasticity tensor and $\boldsymbol{\varepsilon}_{\mathbf{c}}$ is the strain in the continuum caused by the displacement jump across the crack, which is elaborated in the next section.

The cohesive zone damage-healing model relates the crack plane tractions ($\tilde{\boldsymbol{\sigma}}$) to the crack opening displacements ($\tilde{\mathbf{u}}$) through the following relationship:

$$\tilde{\boldsymbol{\sigma}} = \left(1-\omega\right) \cdot \tilde{\mathbf{K}}_{\mathbf{e}} : \tilde{\mathbf{u}} + h \cdot \tilde{\mathbf{K}}_{\mathbf{e}} : \left(\tilde{\mathbf{u}} - \tilde{\mathbf{u}}_{\mathbf{h}} \right), \qquad \forall \mathbf{x} \in \Omega_{crk} \tag{2}$$

in which $\omega \in \left[0,1\right]$ is a scalar damage parameter, $\tilde{\mathbf{K}}_{e}$ is the crack plane stiffness matrix, $h \in \left[0,\omega\right]$ is a scalar healing parameter and $\tilde{\mathbf{u}}_{\mathbf{h}}$ are the crack opening displacements at the time of healing, included in such a way as to ensure the thermodynamic consistency of the healing component of the model (Jefferson and Freeman, 2022).

In the present work, the damage is described using a classical exponential softening relationship that depends on the damage evolution parameter (ζ):

$$\omega = 1 - \frac{u_t}{\zeta} \cdot e^{-c_1 \frac{\zeta - u_t}{u_m - u_t}} \tag{3}$$

126 in which $u_t = f_t h_{cp} / E$, where f_t is the tensile strength of the material, h_{cp} is the crack zone width
127 and E is Young's modulus, $c_1 = 5$ is a softening constant and u_m is the crack opening displacement
128 at the end of the softening curve.

129 The evolution of damage is governed by the following damage function:

130 $$\psi = \zeta_{eq} - \zeta \tag{4}$$

131 where $\zeta_{eq} = \frac{\tilde{u}_1}{2}\left[1+\left(\frac{\mu}{\gamma}\right)^2\right]+\frac{1}{2\gamma^2}\sqrt{\left(\gamma^2-\mu^2\right)^2\tilde{u}_1^2+4\gamma^2\left(\tilde{u}_2^2+\tilde{u}_3^2\right)}$.

132 Damage evolution is subject to the standard Kuhn-Tucker loading conditions:

133 $$\dot{\zeta} \geq 0, \quad \psi \leq 0, \quad \dot{\zeta}\psi = 0 \tag{5}$$

134 in which the superior dot indicates the time derivative.

135 In the present model, healed material is allowed to re-damage and re-heal an unlimited number of
136 times.

137 ## Transport model

138 The governing equations for the crack plane flow are the mass balance equation combined with
139 Darcy's law for the healing agent flux (Freeman and Jefferson, 2020) which, along with boundary
140 conditions, are as follows:

141 $$\begin{aligned}
&\mathbf{v} = -\left(\frac{k_{crk}+0.5\mu w_c \beta_w \beta_{wr}}{\mu}\right)\left(\nabla P_{hcrk} - \rho\mathbf{g}\right), && \forall \mathbf{x} \in \Omega_{crk} \\
&\frac{\partial\left(\rho w_c\right)}{\partial t} + \nabla\cdot\left(\rho w_c \mathbf{v}\right) = 0, && \forall \mathbf{x} \in \Omega_{crk} \\
&P_{hcrk} = P_{Dcrk} = P_c\left(\theta_d\right)\left(1-\beta_s\right) - 2\frac{\beta_m}{w_c}\mathbf{v}\cdot\mathbf{n}, && \forall \mathbf{x} \in \Gamma_f \\
&P_{hcrk} = P_{app}, && \forall \mathbf{x} \in \Gamma_{app}
\end{aligned} \tag{6}$$

142 where Ω_{crk} is the crack domain, Γ_f is the free surface of the healing agent, Γ_{app} is the part of the
143 boundary to which pressure, P_{app}, is applied, $\mathbf{V}$ is the vector of healing agent velocities , P_{hcrk} is the
144 healing agent pressure, w_c is the crack width, μ is the dynamic viscosity and ρ is the density. The
145 crack permeability is given as $k_{crk} = w_c^2/12$, and is derived from Poiseuille flow conditions. β_s and β_m
146 are factors to allow for stick-slip of and frictional dissipation at the meniscus respectively, β_w is a
147 factor to account for wall slip and β_{wr} is the relative wall slip factor (Freeman and Jefferson, 2020).

148 In discrete cracks, the capillary pressure, P_c, is given by the Young-Laplace equation:

149 $$P_c = \frac{2\gamma\cos\left(\theta_d - \psi\right)}{w_c} \tag{7}$$

where γ is the surface tension, ψ is the inclination of the crack wall and θ_d is the dynamic contact angle that is related to the static contact angle (θ_s) through the Jiang et al.'s (Jiang, Soo-Gun and Slattery, 1979) relationship:

$$\tanh\left(c_1 Ca^{c_2}\right) = \frac{\cos\left(\theta_s\right) - \cos\left(\theta_d\right)}{\cos\left(\theta_s\right) + 1} \tag{8}$$

where c_1 and c_2 are constants and $Ca = \mathbf{v} \cdot \mathbf{n}\mu/\gamma$ is the capillary number.

Generalised healing front model

In the present work, the healing agent curing mechanism considered is based on the propagation of a diffuse reaction front, emanating from the crack faces. This process has been shown to be well-described by the following function that is based on an analytical solution of the advection-diffusion equation (Freeman and Jefferson, 2020; Jefferson and Freeman 2022):

$$\xi_x(x,t) = \frac{1}{2}\left(1 - \tanh\left(\left(\frac{2}{\sqrt{\pi}}\right)\left(\frac{x - z(t) - z_c}{z_c + \sqrt{\frac{z(t)}{z_{c1}}}}\right)\right)\right) \tag{9}$$

where $\xi_x(x,t)$ is the degree of cure, z_c is a wall factor, z_{c1} is a diffusion constant and $z(t)$ is a propagation distance that reads:

$$z(t) = z_{c0}\left(1 - e^{-\frac{t}{\tau}}\right) \tag{10}$$

where z_{c0} is a critical curing depth at which the propagation of the front ceases and τ is a characteristic time.

The degree of mechanical healing is given by the degree of cure or relative area of healed material at the centre of the crack:

$$h\left(w_c,t\right) = \frac{1}{2}\left(\left(\frac{f_{stat} + f_{dyn}}{2}\right) - \left(\frac{f_{stat} - f_{dyn}}{2}\right)\tanh\left(\frac{\dot{w}_c - w_{rt}}{w_{rnom}}\right)\right)\left(1 - \tanh\left(\left(\frac{2}{\sqrt{\pi}}\right)\left(\frac{\frac{w_c}{2} - z(t) - z_c}{z_c + \sqrt{\frac{z(t)}{z_{c1}}}}\right)\right)\right) \tag{11}$$

in which $f_{stat} = 1$ and $f_{dyn} = 0.45$ are the static and dynamic factors, $w_{rt} = 10^{-3}\zeta/\tau\ mm/s$ and $w_{rnom} = w_{rt}/10$. The rate term (in the first set of brackets) accounts for the disruption in the propagation of the reaction front arising from significant movement of the crack faces (Jefferson and Freeman, 2022).

3. Numerical implementation

Finite element framework

To solve the coupled system of non-linear equations, we employ the finite element method and a staggered solution method. The governing equation for the transport model is given by Equation 6 and the governing equation for the mechanical model is derived using a conventional virtual work approach. To discretise the crack flow model, we employ the unfitted finite element method of Hansbo and Hansbo (2002), with strong imposition of pressure boundary conditions (Freeman, 2022) and a smooth extension of the solution in elements cut by the healing agent interface to the entire element (Pande, Papadopoulos and Babuška, 2021).

The global system of equations for the mechanical model reads:

$$\mathbf{K}_{\mathbf{g}}\left(\mathbf{u}_{\mathbf{g}}\right)\mathbf{u}_{\mathbf{g}} = \mathbf{F}_{\mathbf{g}}, \qquad \forall \mathbf{x} \in \Omega \tag{12}$$

where $\mathbf{K}_{\mathbf{g}}\left(\mathbf{u}_{\mathbf{g}}\right)$ is the global stiffness matrix, $\mathbf{u}_{\mathbf{g}}$ is the global vector of displacements and $\mathbf{F}_{\mathbf{g}}$ is the global force vector. $\mathbf{K}_{\mathbf{g}}\left(\mathbf{u}_{\mathbf{g}}\right)$ is assembled from element stiffness matrices that take the standard form for uncracked elements and a special form with an embedded strong discontinuity for cracked elements. The non-linearity is dealt with using the Newton-Raphson method.

For the crack plane flow, the global system of equations is given by:

$$\mathbf{K}_{\mathbf{t}}\mathbf{P}_{\mathbf{t}} = \mathbf{F}_{\mathbf{t}}, \qquad \forall \mathbf{x} \in \Omega_{crk} \tag{13}$$

Where $\mathbf{K}_{\mathbf{t}}$ is the global transport system matrix, $\mathbf{P}_{\mathbf{t}}$ is the global vector of pressures and $\mathbf{F}_{\mathbf{t}}$ is the global right hand side vector.

For the crack plane flow, it is necessary to track the movement of the healing agent interface. To this end, we employ the level set method. The level set is a signed distance function whose zero level indicates the interface and, in the present work, a positive value indicates the healing agent domain.

The evolution of the level set function is governed by the following transport problem:

$$\begin{aligned} &\frac{\partial \varphi}{\partial t} + \mathbf{u} \cdot \nabla \varphi = 0, \qquad && \forall \mathbf{x} \in \Omega_{crk} \\ &\varphi(t) = 0, && \forall \mathbf{x} \in \Gamma_{f} \end{aligned} \tag{14}$$

where φ is the level set function.

For the level set method we obtain the following linear system of equations:

$$\mathbf{C}_{\varphi}\partial_{t}\left(\boldsymbol{\varphi}\right) + \mathbf{K}_{\varphi}\boldsymbol{\varphi} = 0, \qquad \forall \mathbf{x} \in \Omega_{crk} \tag{15}$$

For the spatial discretisation we employ the streamline upwind Petrov-Galerkin method (SUPG) where the stabilisation parameter is given as:

$$\tau = 2\left(\frac{1}{\Delta t^{2}} + \frac{\left|\mathbf{u}\cdot\mathbf{u}\right|}{h^{2}}\right)^{-\frac{1}{2}} \tag{16}$$

Whilst we employ an implicit Euler finite difference scheme for the temporal discretisation, we note that re-initialisation is required in order to maintain the level set as a singed distance function. In the present work we employ the modified fast marching method as described in (Groß, Reichelt and Reusken, 2006).

Extension of crack flow solution

The tracking of the fluid interface using the level set method requires the solution in the entire crack plane. As mentioned above, the unfitted finite element method of Hansbo and Hansbo (2002) is employed for the crack plane flow. In this method, the solution is only computed for elements with non-zero intersection with the physical domain (i.e. those that are at least partially filled with healing agent), and as such, the solution needs to be extended. In the present work, the solution is extended using a ghost penalty on the jump in the solution gradient across element edges that reads:

$$\mathbf{j}_p = g_{sp} \sum_{E \in E^G_{crk}} h \int_E \left[\!\left[\nabla \zeta \right]\!\right]_F \left[\!\left[\nabla P_c \right]\!\right]_F \tag{17}$$

where E^G_{crk} is the set of element edges that lie outside of the fluid domain, g_{sp} is a penalty parameter, h is a measure of element size and $\left[\!\left[x \right]\!\right]_F = x_+\big|_F - x_-\big|_F$ is the jump in quantity x across an element edge. We note that this penalty is not required for stabilisation.

Embedded strong discontinuity element

In the present work, the cohesive zone model is applied to an embedded strong discontinuity element, which was presented in 2D form in Freeman et al., (2020). Here, we present the derivation of the new 3D hexahedral element that contains an embedded plane discontinuity. A depiction of the element that shows the inelastic components of crack opening displacements ($\breve{\mathbf{u}}$), crack rotations ($\boldsymbol{\alpha}$) and crack plane local axes ($\mathbf{r}$), can be seen in Figure 1.

The discontinuity representing the crack splits the element into two subdomains, Ω_{K}^- and Ω_{K}^+ such that $\Omega_{\mathrm{K}} = \Omega_{\mathrm{K}}^- \cup \Omega_{\mathrm{K}}^+$ where Ω_{K} is the element domain. Using the Heaviside function, H, the element displacements can be split into a continuum part, $\mathbf{u}_{\mathrm{e}}$, and the displacement jump associated with the crack, $\mathbf{u}$, giving:

$$\mathbf{u}(\mathbf{x},t) = \mathbf{u}_{\mathrm{e}}(\mathbf{x},t) + H\left[\!\left[\mathbf{u} \right]\!\right](\mathbf{x},t) \tag{18}$$

In the present work, the displacement jumps associated with the crack are stored in a crack plane vector that contains the crack opening and sliding displacements, as well as rotations about the local crack plane axes, at the centre of the crack:

$$\breve{\mathbf{w}} = \left[\breve{u}_{1,C}, \breve{u}_{2,C}, \breve{u}_{3,C}, \breve{\alpha}_1, \breve{\alpha}_2, \breve{\alpha}_3 \right] \tag{19}$$

where $\breve{\mathbf{u}}$ is the inelastic component of the local relative displacement vector. The elastic part, $\tilde{\mathbf{u}}_e$, is associated with an elastic band of material on either side of the discontinuity and arises as a result of the treatment of the crack plane as a narrow band of material of finite width.

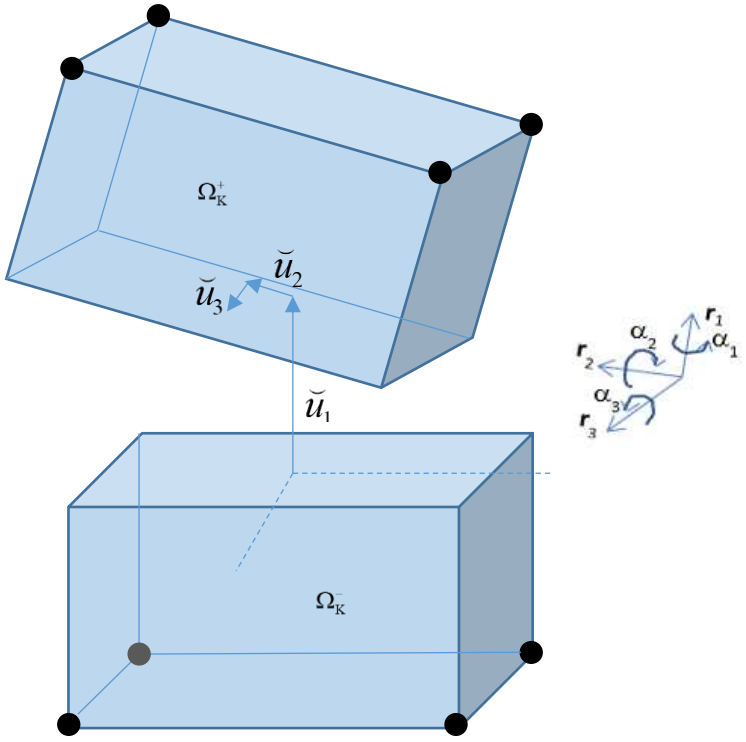

Figure 1 – Eight-noded hexahedral element with an embedded discontinuity

The opening and sliding displacements can be obtained at any position within the crack, $\left(r_2, r_3\right)$, from the crack plane vector as follows:

$$\mathbf{u}_{cp}\left(r_2, r_3\right) = \begin{bmatrix} 1 & 0 & 0 & 0 & r_3 & -r_2 \\ 0 & 1 & 0 & -r_3 & 0 & 0 \\ 0 & 0 & 1 & r_2 & 0 & 0 \end{bmatrix} \breve{\mathbf{w}}^T = \mathbf{\Lambda}\breve{\mathbf{w}}^T \tag{20}$$

The displacement in the positive part of the element, due to the relative displacement across the discontinuity, is given by the following mapping of the rigid body motion:

$$\mathbf{u}_c\left(\mathbf{x}\right) = H\left(\mathbf{x}\right) \begin{bmatrix} r_{1,1} & r_{2,1} & r_{3,1} & \left(r_{1,2}\Delta x_3 - r_{1,3}\Delta x_2\right) & \left(r_{2,2}\Delta x_3 - r_{2,3}\Delta x_2\right) & \left(r_{3,2}\Delta x_3 - r_{3,3}\Delta x_2\right) \\ r_{1,2} & r_{2,2} & r_{3,2} & \left(r_{1,3}\Delta x_1 - r_{1,1}\Delta x_3\right) & \left(r_{2,3}\Delta x_1 - r_{2,1}\Delta x_3\right) & \left(r_{3,3}\Delta x_1 - r_{3,1}\Delta x_3\right) \\ r_{1,3} & r_{2,3} & r_{3,3} & \left(r_{1,1}\Delta x_2 - r_{1,2}\Delta x_1\right) & \left(r_{2,1}\Delta x_2 - r_{2,2}\Delta x_1\right) & \left(r_{3,1}\Delta x_2 - r_{3,2}\Delta x_1\right) \end{bmatrix} \breve{\mathbf{w}}^T$$
$$= \mathbf{T}_w\left(\mathbf{x}\right)\breve{\mathbf{w}}^T \tag{21}$$

in which $\Delta\mathbf{x} = \mathbf{x} - \mathbf{x}_c$, where $\mathbf{x}_c$ are the coordinates of the crack plane centre.

The force vector across the crack plane is obtained by integrating the crack plane tractions as follows:

248 $$\tilde{\mathbf{F}} = \begin{bmatrix} \tilde{\mathbf{F}}_{r1} \\ \tilde{\mathbf{F}}_{r2} \\ \tilde{\mathbf{F}}_{r3} \\ \tilde{\mathbf{M}}_{r1} \\ \tilde{\mathbf{M}}_{r2} \\ \tilde{\mathbf{M}}_{r3} \end{bmatrix} = \begin{bmatrix} \int_A (\tilde{\sigma}_{r1})\, dA \\ \int_A (\tilde{\sigma}_{r2})\, dA \\ \int_A (\tilde{\sigma}_{r3})\, dA \\ \int_A (-\tilde{\sigma}_{r2} r_3 + \tilde{\sigma}_{r3} r_2)\, dA \\ \int_A (\tilde{\sigma}_{r1} r_3)\, dA \\ \int_A (-\tilde{\sigma}_{r1} r_2)\, dA \end{bmatrix} \quad (22)$$

249 where the integrals are evaluated using a summation over local crack plane triangular elements.

250 Using Equation (22) and the constitutive relation given in Equation (2), the relationship between the
251 crack plane displacement and force vectors can be derived as:

252 $$\tilde{\mathbf{F}} = \tilde{\mathbf{K}}\tilde{\mathbf{w}} + \tilde{\mathbf{K}}_h (\tilde{\mathbf{w}} - \tilde{\mathbf{w}}_h) \quad (23)$$

253 The elastic crack plane stiffness matrix is given by:

254 $$\tilde{\mathbf{K}}_e = \begin{bmatrix} \int_A (k_r)\, dA & 0 & 0 & 0 & \int_A (k_r r_3)\, dA & \int_A (-k_r r_2)\, dA \\ 0 & \int_A (k_s)\, dA & 0 & \int_A (-k_s r_3)\, dA & 0 & 0 \\ 0 & 0 & \int_A (k_s)\, dA & \int_A (k_s r_2)\, dA & 0 & 0 \\ 0 & \int_A (-k_s r_3)\, dA & \int_A (k_s r_2)\, dA & \int_A \left(k_s \left(r_2^2 + r_3^2 + 2 r_2 r_3\right)\right) dA & 0 & 0 \\ \int_A (k_r r_3)\, dA & 0 & 0 & 0 & \int_A \left(k_r r_3^2\right) dA & \int_A (-k_r r_2 r_3)\, dA \\ \int_A (-k_r r_2)\, dA & 0 & 0 & 0 & \int_A (-k_r r_2 r_3)\, dA & \int_A \left(k_r r_2^2\right) dA \end{bmatrix}$$

255 (24)

256 We note that $\tilde{\mathbf{K}}$ and $\tilde{\mathbf{K}}_h$ are defined similarly with each term within the integrals being multiplied
257 by $(1-\omega)$ and h respectively.

258 The strain in the continuum due to the discontinuity can be obtained as follows:

259 $$\boldsymbol{\varepsilon}_{\mathbf{c}} = \mathbf{M}_w \tilde{\mathbf{w}}^{\mathbf{T}} + \mathbf{M}_h \tilde{\mathbf{w}}_h^{\mathbf{T}} \quad (25)$$

260 in which $\mathbf{M}_w = \mathbf{B}(\mathbf{x})\mathbf{T}_{\mathbf{w}}(\mathbf{x})\left(\mathbf{I}_6 - \tilde{\mathbf{K}}_e^{-1}\left(\tilde{\mathbf{K}} + \tilde{\mathbf{K}}_h\right)\right)$, where $\mathbf{B}(\mathbf{x})$ is the standard strain displacement
261 matrix and $\mathbf{I}_6$ is the rank 6 identity matrix, and $\mathbf{M}_h = \tilde{\mathbf{K}}_e^{-1}\tilde{\mathbf{K}}_h$.

262 Using Equation (25) and noting that an increment of healing does not alter the stress state, the virtual
263 work equation can be written as (Freeman *et al.*, 2020):

264 $$\begin{aligned} \delta\Pi_e = \int_{\Omega_e} \left(\delta\mathbf{u}_e^T\mathbf{B}^T - \delta\tilde{\mathbf{w}}^T\mathbf{M}_w^T\right)\mathbf{D}\left(\mathbf{B}\mathbf{u}_e - \mathbf{M}_w\tilde{\mathbf{w}} - \mathbf{M}_h\tilde{\mathbf{w}}_h\right) d\Omega_e + \delta\tilde{\mathbf{w}}^T\left(\tilde{\mathbf{K}}_{ww}\tilde{\mathbf{w}} - \tilde{\mathbf{K}}_{wh}\tilde{\mathbf{w}}_h\right) \\ -\delta\mathbf{u}_e^T\mathbf{F}_e = 0 \end{aligned} \quad (26)$$

where $\tilde{\mathbf{K}}_{ww} = \left(\mathbf{I}_6 - \tilde{\mathbf{K}}_e^{-1}\left(\tilde{\mathbf{K}} + \tilde{\mathbf{K}}_h\right)\right)^T \left(\tilde{\mathbf{K}} + \tilde{\mathbf{K}}_h\right)$ and $\tilde{\mathbf{K}}_{wh} = \left(\mathbf{I}_6 - \tilde{\mathbf{K}}_e^{-1}\left(\tilde{\mathbf{K}} + \tilde{\mathbf{K}}_h\right)\right)^T \left(\tilde{\mathbf{K}}_h\right)$.

Enforcing equilibrium between the tractions and stresses in the crack plane and continuum respectively in a weak sense, we obtain the following relationship:

$$\begin{aligned}\tilde{\mathbf{w}} &= \left(\left[\int_{\Omega_e} \mathbf{M}_w^T \mathbf{D} \mathbf{M}_w d\Omega_e + \tilde{\mathbf{K}}_{ww}\right]^{-1} \int_{\Omega_e} \mathbf{M}_w^T \mathbf{D} \mathbf{B} d\Omega_e\right)\mathbf{u}_e + \left(\int_{\Omega_e} -\mathbf{M}_w^T \mathbf{D} \mathbf{M}_h d\Omega_e + \tilde{\mathbf{K}}_{wh}\right)\tilde{\mathbf{w}}_h \\ &= \mathbf{C}_u \mathbf{u}_e + \mathbf{C}_h \tilde{\mathbf{w}}_h\end{aligned} \tag{27}$$

Employing (27) in Equation (26), the following element stiffness matrix relationship is derived:

$$\mathbf{K}_{SDeh}\mathbf{u}_e = \mathbf{F}_e + \mathbf{K}_{eh}\tilde{\mathbf{w}}_h \tag{28}$$

where:

$$\begin{aligned}\mathbf{K}_{SDeh} &= \int_{\Omega_e} \left(\mathbf{B}^T - \mathbf{C}_u^T \mathbf{M}_w^T\right)\mathbf{D}\left(\mathbf{B} - \mathbf{M}_w \mathbf{C}_u\right) d\Omega_e + \mathbf{C}_u^T \tilde{\mathbf{K}}_{ww} \mathbf{C}_u \\ \mathbf{K}_{eh} &= \int_{\Omega_e} \left(\mathbf{B}^T - \mathbf{C}_u^T \mathbf{M}_w^T\right)\mathbf{D}\left(\mathbf{M}_w \mathbf{C}_h - \mathbf{M}_h\right) d\Omega_e - \left(\mathbf{C}_u^T \tilde{\mathbf{K}}_{ww} \mathbf{C}_h - \tilde{\mathbf{K}}_{wh}\right)\end{aligned} \tag{29}$$

Crack tracking

In order to ensure crack continuity, we employ a 3D version of the crack tracking algorithm of Alfaiate et al. (2002; 2003), whilst U-turns in the crack path were prevented using the approach of Cervera et al. (2010). In elements for which there are no crack tips on the element faces, the crack is assumed to cross through the centroid of the element, with the orientation being governed by the direction of the maximum principal strain. For elements that have a crack tip on one of the element faces, the crack is assumed to start from the existing crack tip and the orientation is governed by the direction of the maximum principal strain. Finally, for elements that have crack tips on multiple faces, the crack is assumed to connect the existing crack tips.

Coupling between mechanical and transport model

An important aspect of the formulation is the coupling between the mechanical and transport components of the model. In the present work, there is a two-way coupling between these components, which reflects the physical processes that govern the self-healing response. The effect of the mechanical response on the healing agent transport is accounted for through both the crack opening displacements (crack widths) and crack opening displacement rate, as can be seen from Equation (6). The mechanical response is dependent on the amount of agent available for healing. In the model, this is accounted for in the healing variable update, where the area available for healing is dependent on the degree of damage and the relative crack filling predicted by the transport model. The healing variable update employs the method described in Jefferson and Freeman (2022), as follows:

$$\begin{aligned}\Delta a &= \Delta\omega r_{fill} + a_{i\text{-}1}\Delta r_{fill} \\ a_{v_i} &= a_{v_{i\text{-}1}} + \Delta a \\ a_i &= a_{v_i} - a_{red} + a_{rec} r_{fill}\end{aligned} \tag{30}$$

in which a is the relative area (termed area hereafter) available for healing, $a_{red} = \omega_{h_{i1}} h_{v_{i\text{-}1}}$ is the re-damaged area, where $\omega_{h_{i1}}$ is the degree of damage of healed material and $h_{v_{i\text{-}1}}$ is the virgin healing

variable, $a_{rec} = a_{red} r_{fill}$ is the area of a_{red} that has been re-filled and r_{fill} is the degree of crack filling that is calculated from the transport model. The link between the area available for healing and the mechanical regain is found in the calculation of the degree of healing, through the healing front variable, z (noting that $h(z)$), which is updated as follows:

$$z_i = z_r e^{-\Delta t/\tau} + z_{c0} a_i \left(1 - e^{-\Delta t/\tau}\right) \tag{31}$$

As the crack plane integrations are carried out over sub-triangles, a value of r_{fill} is calculated for each sub-triangle from the level set function. A depiction of a sub-triangulated crack plane, and associated level set can be seen in Figure 2.

To calculate the filling area, we first employ an inverse isoparametric mapping to obtain the crack plane centre in the local coordinate system, as detailed in Li, Wittek and Miller (2014). Following this, we then find the coordinates of the intersections of the level set with the sub-triangle edges, before the area for each is calculated using Gauss' area formula.

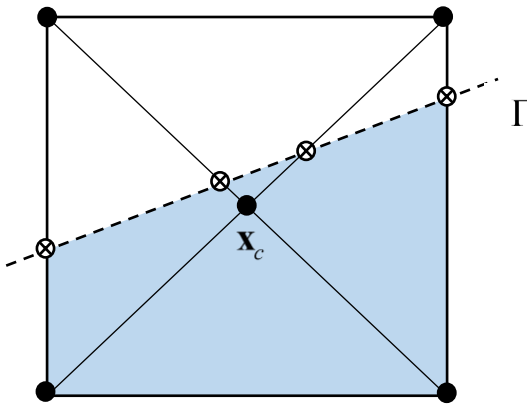

Figure 2 – Crack plane showing sub-triangulation and healing agent interface, marked by the dashed line, where the shaded region indicates the healing agent domain, the sub-triangle corners are indicated by the black circles and the points of intersection between the level set and the sub-triangles are indicated by the crossed circles

4. Example problems

In this section we consider example problems to demonstrate the performance of the model. The first set of problems considers the healing front model. This model (presented in Section 2) was originally developed to describe the propagation of curing fronts in cyanoacrylate adhesives. Two problems are considered that show the generality of the model and its applicability to other healing mechanisms in which curing, or precipitation of healing material, starts at the crack faces. The next example problem considers the mechanical response of a cementitious specimen with embedded vascular networks and a SS healing agent. The penultimate example concerns the autogenous healing of a cementitious specimen with and without CA that are introduced to stimulate healing. In the final example, the mechanical response of a vascular self-healing slab with SS is considered. For these simulations, we assume that the rate of molecular diffusion of the chemical species is negligible relative to both the chemical reaction rates and the rate of liquid transport. The extension of the healing model to include chemical species transport in the crack is the subject of future work. The model parameters used in the latter three analyses can be seen in Tables 1 & 2, where the subscript h indicates healed material.

328 Table 1 – Mechanical model parameters

Parameter	Example			
	2	**3a**	**3b**	**4**
E, E_h (N/mm^2)	30 000	20 000	20 000	30 000
ν, ν_h (-)	0.2	0.2	0.2	0.2
f_t (N/mm^2)	3.7	1.0	1.0	3.7
f_{th} (N/mm^2)	2.0	0.5	0.5	2.0
u_t (mm)	0.110	0.175	0.175	0.110
u_{th} (mm)	0.060	0.200	0.120	0.060
τ (days)	21	135	270	21
z_{c0} (mm)	0.05	0.05	0.05	0.05
z_{c1} (mm)	25	25	25	25
E_s (N/mm^2)	-	-	-	200 000
f_{tsu} (N/mm^2)	-	-	-	850
H_s (N/mm^2)	-	-	-	5 000

329 *where E_s and f_{tsu} are the Young's modulus and ultimate tensile strength of steel and H_s is the
330 hardening stiffness
331 **3a refers to the case with CA, whilst 3b refers to that without

332 Table 2 – Transport model parameters

Parameter	Example			
	2	**3a**	**3b**	**4**
μ (Ns/m^2)	0.1	0.1	0.1	0.1
θ_s (rad)	0.1754	0.1754	0.1754	0.1754
c_1 (-)	1.325	1.325	1.325	1.325
c_2 (-)	0.35	0.35	0.35	0.35
γ (N/m)	0.0728	0.0728	0.0728	0.0728
ρ (kg/m^3)	1840	1000	1000	1840
β_w (m^3/Ns)	0	0	0	0
β_s (-)	0	0	0	0
β_m (Ns/m^2)	0	0	0	0
P_{app} (N/m^2)	20 000	0	0	5 000

333

334

Example 1. Healing front study

The first healing front study concerns healing through microbially induced calcite precipitation and considers a set of tests undertaken by Xin et al. (2020). In Xin et al's experiments, porous ceramic specimens of dimension 24mm × 8mm × 2mm were prepared, before being soaked in solution containing bacteria for 24 hours. Following this, the specimens were broken in half using three-point bending and the two halves fixed together leaving a crack of 300 µm width. The fixed specimens were then immersed in a urea-$CaCl_2$ solution for 14 days, with scanning electron microscopy images taken of the area coverage ratio of calcite pillars bridging the crack every two days during this healing period. The model material parameters are given Table 3. A comparison of the predictions of the healing front model with the experimental data can be seen in Figure 3.

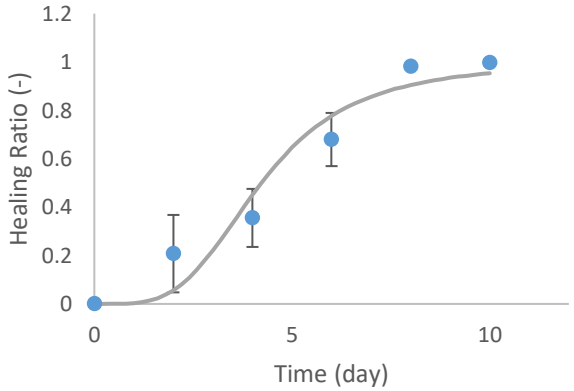

Figure 3 – Comparison between healing front model (solid line) and experimental data (markers) for healing ratio at the centre of a crack

Table 3 – Healing front model parameters MICP

Parameter	Value
z_{c0} (mm)	1
z_{c1} (mm)	20
z_{c2} (mm)	0.00001
τ (days)	26

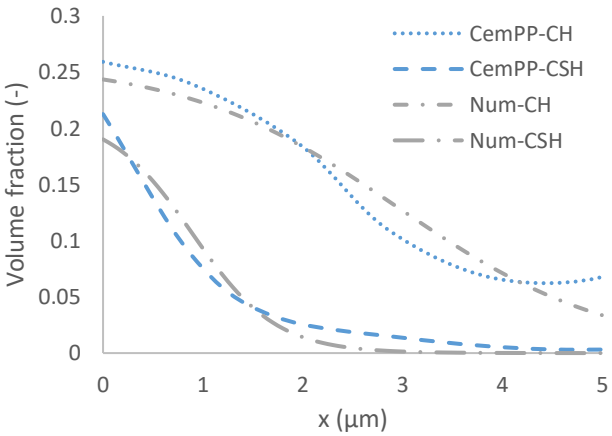

Figure 4 – Comparison between healing product profiles predicted by the healing front model and cement hydration model CemPP

Figure 3 shows that the model gives a good prediction of the experimental behaviour.

The second problem concerns autogenous healing due to further hydration, and considers an example presented in Hilloulin et al. (2016). As part of their study, the authors employed a modified version of the CemPy model (based on CEMHYD3D (Bentz, 1997)) called CemPP, in order to simulate the healing response. Using the model, the authors investigated the distribution of healing products within a 10 µm crack in a 7 day old cement paste specimen. The model parameters used for the analysis are given in Table 4. A comparison of profiles of calcium hydroxide (CH) and calcium-silicate-hydrate (CSH) from the healing front model fitted with the results of the cement hydration model can be seen in Figure 4.

Table 4 – Healing front model parameters further hydration

Parameter (CH)	**Value (CH)**	**Parameter (CSH)**	**Value (CSH)**
z_{c0} (µm)	10	z_{c0} (µm)	2.4
z_{c1} (µm)	0.5	z_{c1} (µm)	1
z_{c2} (µm)	0.00001	z_{c2} (µm)	0.00001
τ (days)	20	τ (days)	15

It may be seen from the figure that the healing front model is in good agreement with the results of the cement hydration model.

Example 2. Three-point bending vascular self-healing specimen

In this example, we consider the three-point bending of a cementitious specimen with an embedded vascular network presented in (Davies, Jefferson and Gardner, 2021). The test set up and specimen dimensions are shown in Figure 5. The specimen was loaded in three-point bending until a crack mouth opening displacement (CMOD) of 0.3 mm was reached, after which the specimen was unloaded, left submerged in water for a healing period of one week, before being reloaded to failure. The finite element mesh employed is given in Figure 6. The mesh comprised 1950 elements, whilst the load was applied in 53 increments.

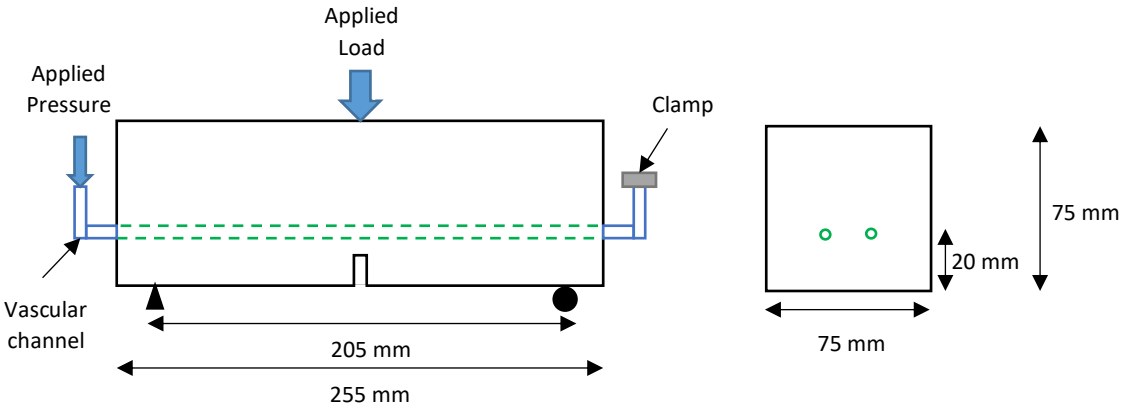

Figure 5 – Test set up and specimen dimensions left) elevation and right) cross-section

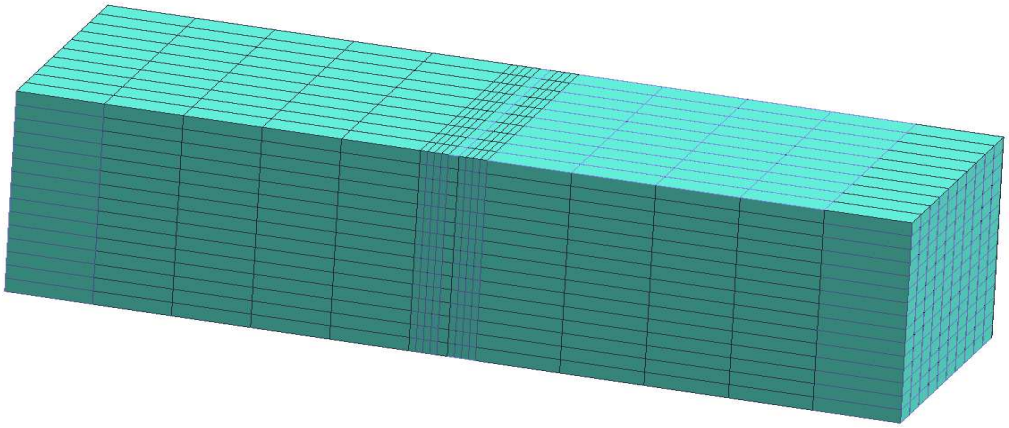

Figure 6 – Finite element mesh

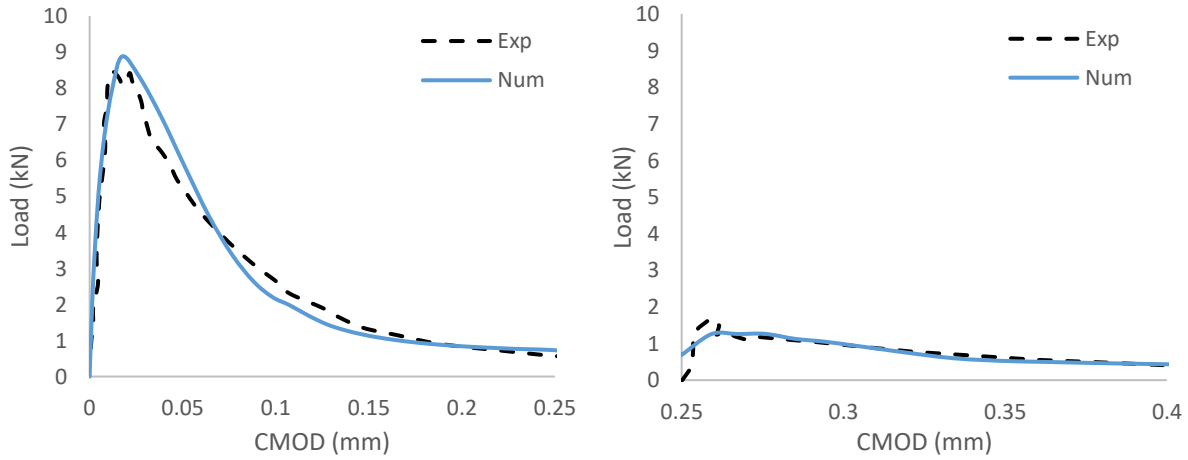

Figure 7 – Comparison of load response left) Pre-cracking and right) Post-healed response

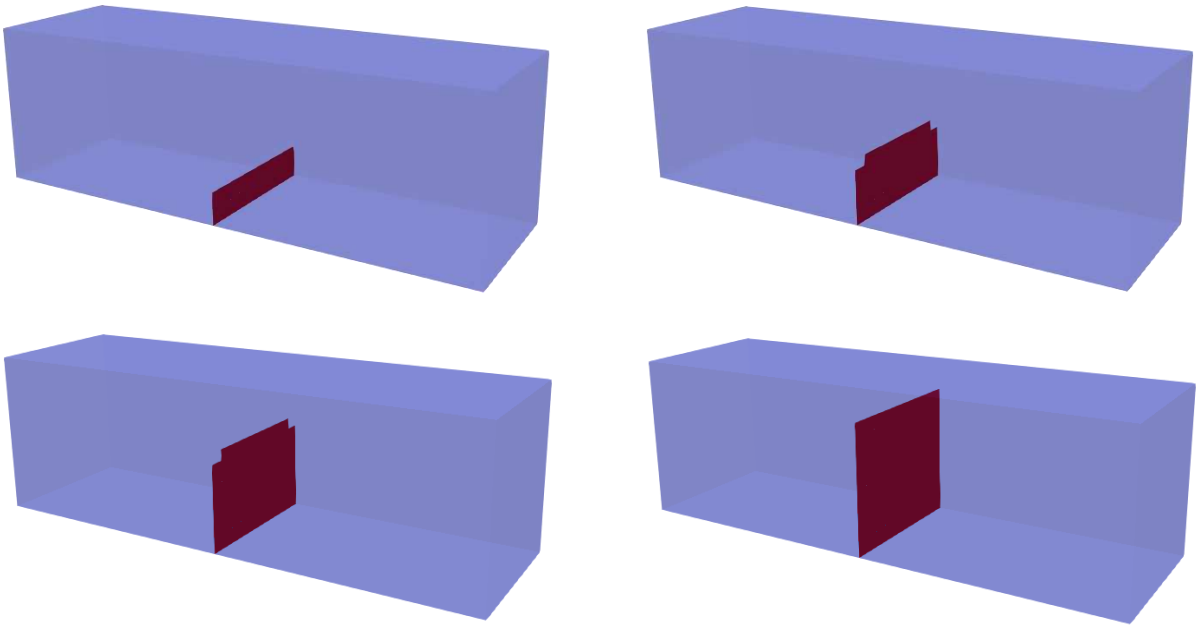

Figure 8 – Predicted crack pattern at displacements of top left) 0.0025 mm, top right) 0.0083 mm, bottom left) 0.0206 mm and bottom right) 0.0544 mm

The comparison between the numerical simulations and the experimental data is given in Figure 7. It can be seen from the figure that the numerical model is able to accurately reproduce the experimental data in terms of both the pre-cracking and post-healed response. The growth of the crack as predicted by the numerical model is shown in Figure 8. It may be seen from the figure that in the early and later stages of loading, the crack is uniform across the width of the specimen, but in the intermediate stage (corresponding to a vertical displacement of 0.0083-0.0206 mm), the outer edges of the crack front are lower than that in the central portion. Contours showing the final displacements at the end of the test are given in Figure 9.

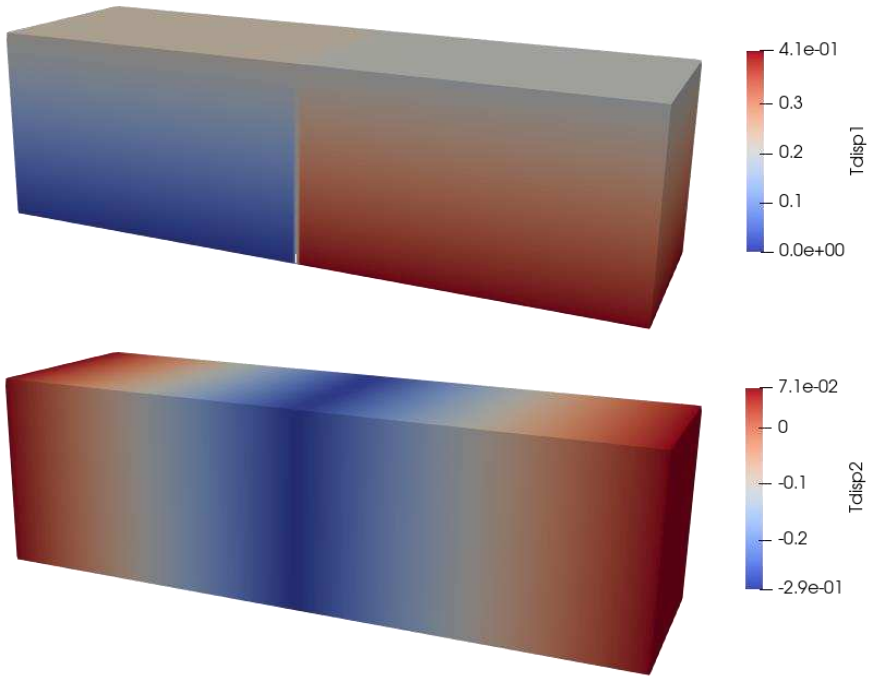

Figure 9 – Contour of final displacements in top) x and bottom) y

Example 3. Autogenous healing with and without crystalline admixtures

In this example, we consider the three-point bending of the cementitious specimens presented in Ferrara, Krelani and Carsana (2014), which have been simulated by Cibelli et al. (2022). The original tests series explored the effect of adding crystalline admixtures (CAs) to the cementitious mix on the degree of autogenous healing. The test set up and specimen dimensions are shown in Figure 10. The specimen was loaded in three-point bending until a crack mouth opening displacement (CMOD) of 0.3 mm was reached, after which the specimen was unloaded. The specimen was then left submerged in water for a range of healing periods, before being reloaded to failure. The finite element mesh employed can be seen in Figure 11. The mesh comprised of 12320 elements, whilst the load was applied in 56 increments.

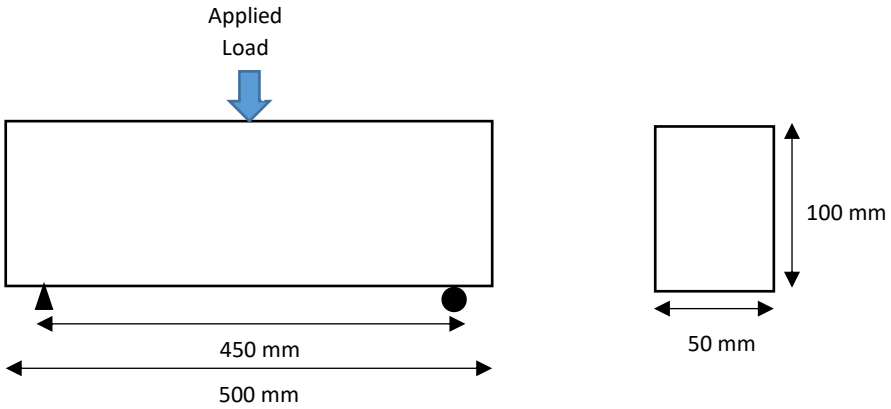

404
405 Figure 10 – Test set up and specimen dimensions

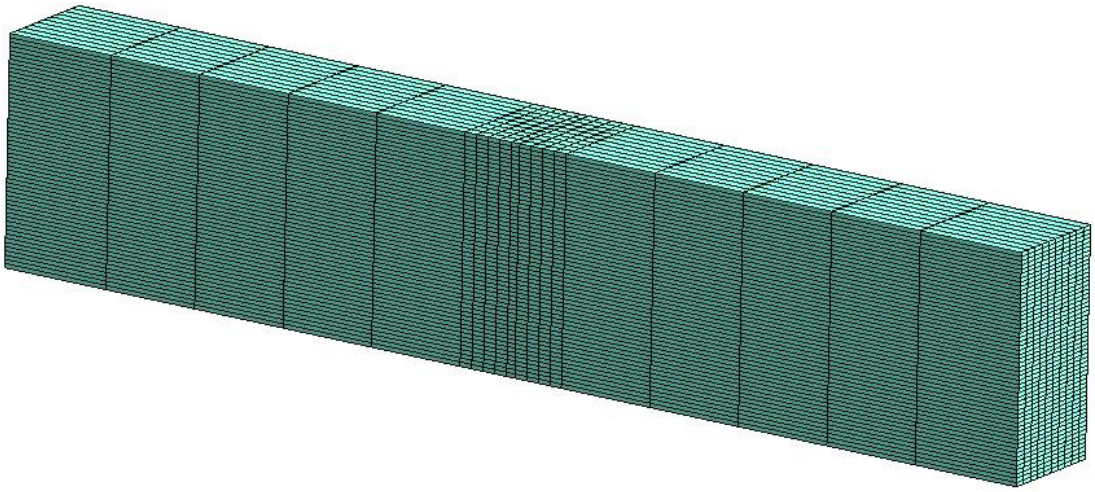

406
407 Figure 11 – Finite element mesh

408 Comparisons between the results from the numerical simulations and the experimental data are given
409 in Figure 12. It can be seen from the figure that the numerical model is able to accurately reproduce
410 the experimental data in terms of the pre-cracking response. The figure also shows that the numerical
411 simulations are able to capture the post-healed response. The largest discrepancies are in the post-
412 healed peak load and initial reloading stiffness. The reason for these differences is thought to relate
413 to residual stresses and crack-opening displacements present in the sample in the unloading phase
414 and associated creep behaviour. The numerical model does not account for this and as such, the
415 residual strength and stiffness is that of the sample at the point of unloading. However, the predicted
416 post-healed peak loads are in good agreement with the results of Cibelli et al. (2022). The growth of
417 the crack -as predicted by the numerical model- is shown in Figure 13. Finally, contours that show the
418 displacements at the end of the test are shown in Figure 14.

419

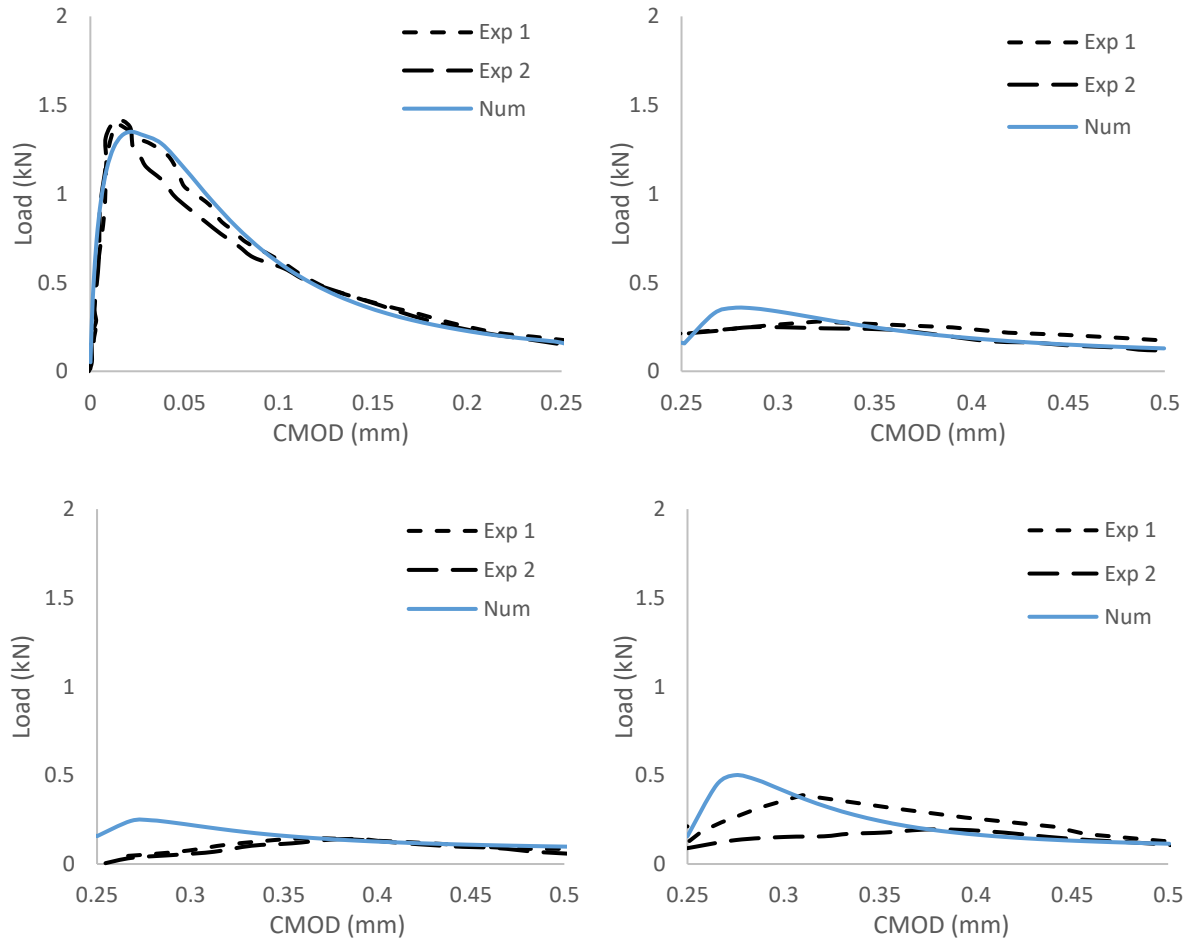

Figure 12 – Comparison of load response top left) Pre-cracking, top right) Post-healed response with CA and 3 months healing period, bottom left) Post-healed response without CA and 3 months healing period and bottom right) Post-healed response without CA and 12 months healing period

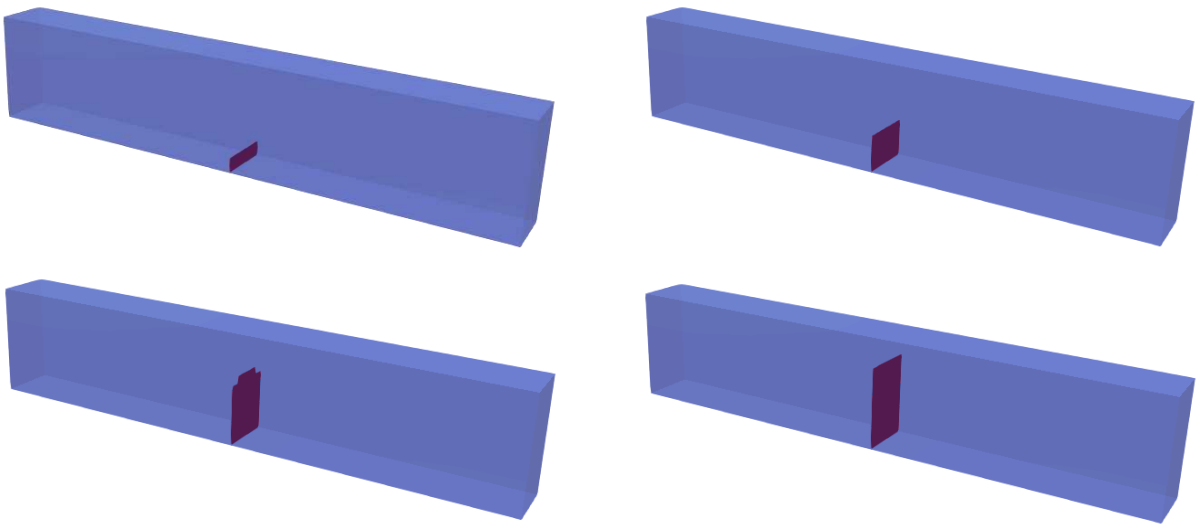

Figure 13 – Predicted crack pattern at displacements of top left) 0.0022 mm, top right) 0.0073 mm, bottom left) 0.0178 mm and bottom right) 0.0337 mm

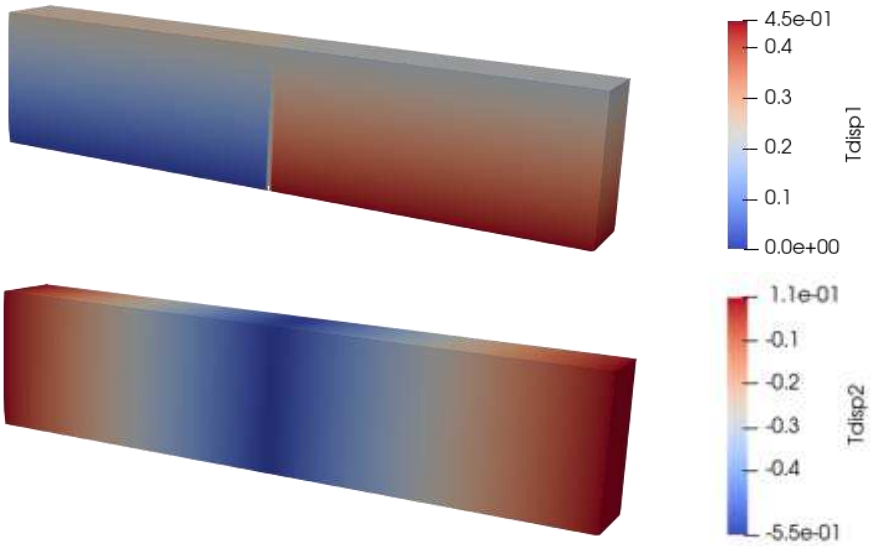

Figure 14 – Contour of displacements in x and y after final load increment

Example 4. Vascular self-healing slab

The final example concerns the loading of a concrete slab with an embedded vascular network presented in (Davies, Jeffersons and Gardner, 2021). The test set up and specimen dimensions are shown in Figure 15. A concentrated patch load was applied to the upper surface of the slab in the centre of the specimen until a central displacement of 6 mm was reached, after which the specimen was unloaded, covered in a moist hessian sack for a healing period of 28 days, and then reloaded to failure. The finite element mesh employed is shown in Figure 16. The mesh comprised 10571 elements and the load was applied in 42 increments. The steel reinforcement was assumed to be perfectly bonded to the concrete and was simulated using a 1D elastic strain-hardening plastic material model. Due to the symmetry of the problem, one quarter of the domain was simulated.

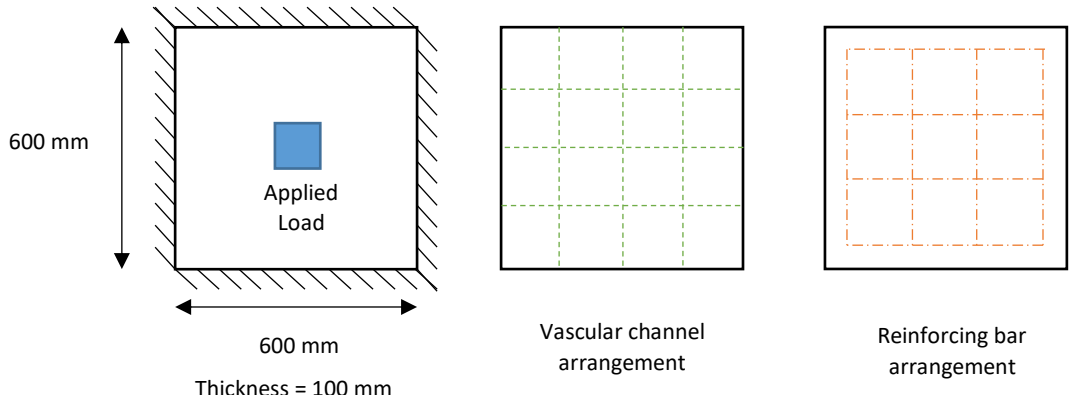

Figure 15 – Test set up and specimen dimensions

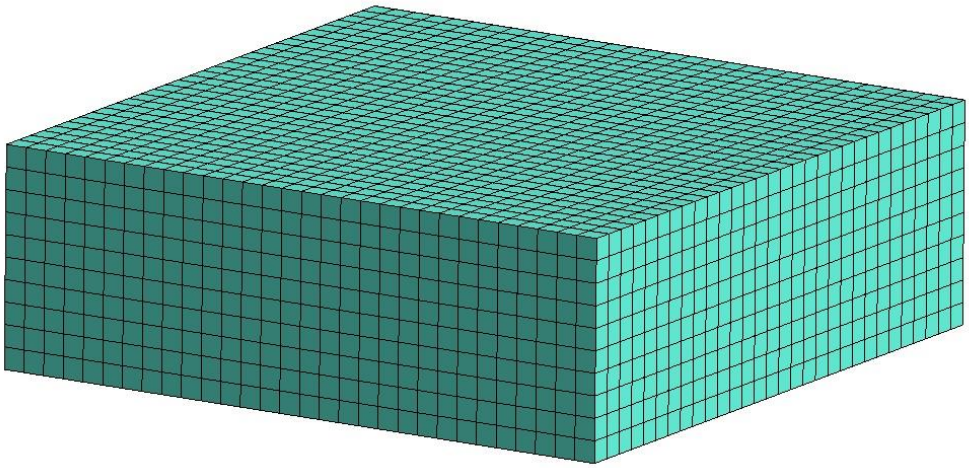

Figure 16 – Finite element mesh

The comparison between the numerical simulations and the experimental data is given in Figure 17. It can be seen from the figure that the numerical model is able to accurately reproduce the experimental data in terms of both the pre-cracking and post-healed response. For the post-healed response, the experimental data show a load increase of just 2 % due to healing. In general, strength and stiffness gains in reinforced samples are very much lower than in unreinforced specimens because the degree of mechanical healing is masked by the presence of reinforcement (Tsangouri *et al.*, 2019). In addition, in reinforced specimens larger crack widths are reached for which healing may be limited (Tsangouri *et al.*, 2019). Figure 18 shows that the numerical and experimental crack patterns are similar. A contour plot showing the vertical displacement at the end of the pre-cracking phase is given in Figure 19.

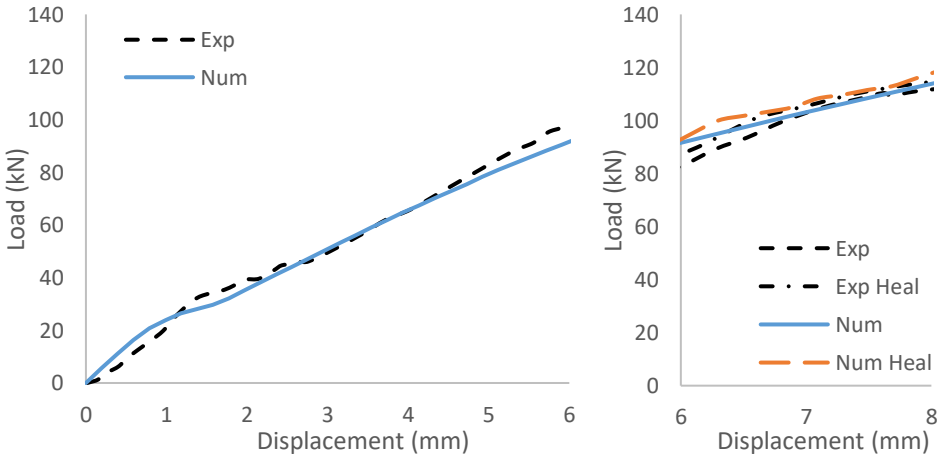

Figure 17 – Comparison of load response left) Pre-cracking and right) Post-healed response

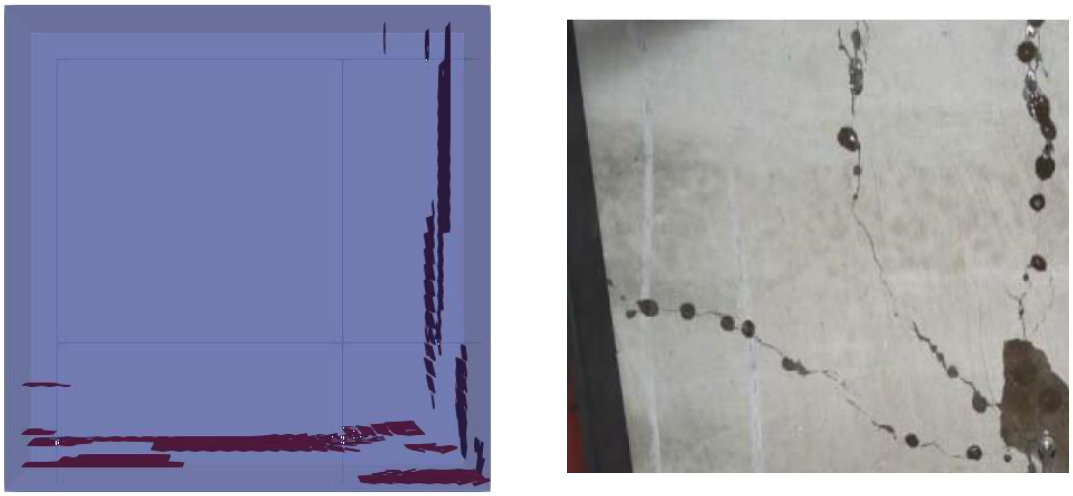

Figure 18 – Predicted crack pattern left) Numerical predictions and right) Experimental after (Davies, Jefferson and Gardner, 2021)

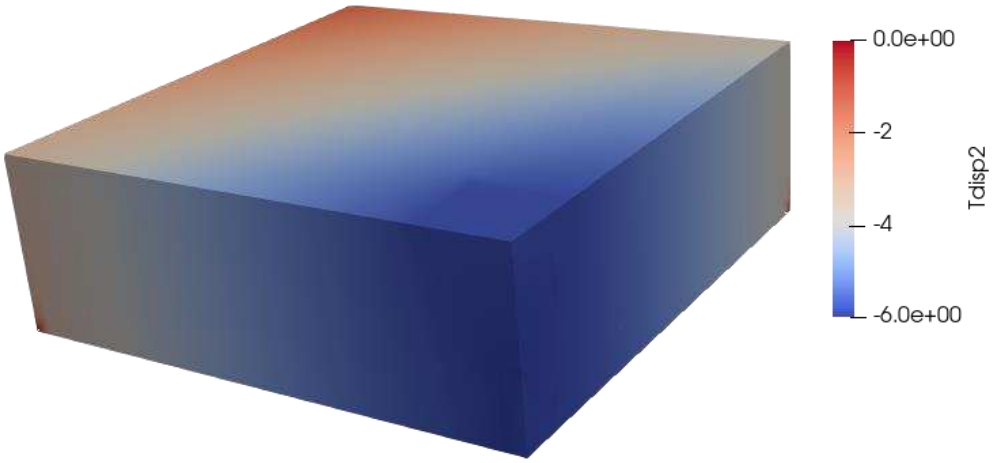

Figure 19 – Contour of y displacement after pre-cracking phase

5. Concluding remarks

In this study, a new 3D coupled finite element model for simulating the behaviour of self-healing cementitious materials has been presented. Based on the results of this work, the following conclusions can be drawn:

- the new embedded strong discontinuity hexahedral element is an effective means of representing discrete cracks and healing in three dimensions:
- the effect of the cracking behaviour on the healing agent transport is naturally accounted for by the crack-width dependent discrete crack flow relationships:
- the proposed crack filling function provides an effective means of accounting for the amount of agent available for healing:
- the generalised curing front model is able to accurately simulate the accumulation of healed material within the cracks for a range of agents:
- the degree of healing of a discrete crack may be computed with good accuracy from the overlap of curing fronts emanating from opposing crack faces:

- the new coupled model, originally developed for a vascular system with cyanoacrylate as the healing agent, is applicable to a wider-range of healing materials including sodium silicate solution and autogenous agents enhanced by the presence of crystalline admixtures.

Data Availability Statement

Some or all data, models, or code generated or used during the study are available in a repository online in accordance with funder data retention policies.
Information on the data underpinning the results presented here, including how to access them, can be found in the Cardiff University data catalogue at (https://doi.org/10.17035/d.2022.0217821360).

Acknowledgements

Financial support from the EPSRC Grant EP/P02081X/1 “Resilient materials for life (RM4L)” is gratefully acknowledged.

References

Alfaiate, J., Simone, A. and Sluys, L. J. (2003) ‘Non-homogeneous displacement jumps in strong embedded discontinuities’, *International Journal of Solids and Structures*, 40(21), pp. 5799–5817. doi: 10.1016/S0020-7683(03)00372-X.

Alfaiate, J., Wells, G. N. and Sluys, L. J. (2002) ‘On the use of embedded discontinuity elements with crack path continuity for mode-I and mixed-mode fracture’, *Engineering Fracture Mechanics*, 69(6), pp. 661–686. doi: 10.1016/S0013-7944(01)00108-4.

Aliko-Benítez, A., Doblaré, M. and Sanz-Herrera, J. A. (2015) ‘Chemical-diffusive modelling of the self-healing behavior in concrete’, *International Journal of Solids and Structures*, 70, pp. 392–402. doi: 10.1016/j.ijsolstr.2015.05.011.

Barbero, E. J., Greco, F. and Lonetti, P. (2005) ‘Continuum Damage-healing Mechanics with Application to Self-healing Composites’, *International Journal of Damage Mechanics*.

De Belie, N. *et al.* (2018) ‘A review of self-healing concrete for damage management of structures’, *Advanced Materials Interfaces*.

Bentz, D. P. (1997) ‘Three-dimensional computer simulation of portland cement hydration and microstructure development’, *Journal of the American Ceramic Society*, 80(1), pp. 3–21.

van Breugel, K. (1995) ‘Numerical simulation of hydration and microstructural development in hardening cement-based materials (I) theory’, *Cement and Concrete Research*, 25(2), pp. 319–331. doi: 10.1016/0008-8846(95)00017-8.

Cervera, M. *et al.* (2010) ‘A crack-tracking technique for localized damage in quasi-brittle materials’, *Engineering Fracture Mechanics*. Elsevier Ltd, 77(13), pp. 2431–2450. doi: 10.1016/j.engfracmech.2010.06.013.

Chitez, A. S. and Jefferson, A. D. (2016) ‘A coupled thermo-hygro-chemical model for characterising autogenous healing in ordinary cementitious materials’, *Cement and Concrete Research*. Elsevier Ltd, 88, pp. 184–197. doi: 10.1016/j.cemconres.2016.07.002.

Cibelli, A. *et al.* (2022) ‘A discrete numerical model for the effects of crack healing on the behaviour of ordinary plain concrete: Implementation, calibration, and validation’, *Engineering Fracture Mechanics*, 263, p. 108266. doi: https://doi.org/10.1016/j.engfracmech.2022.108266.

Cusatis, G., Pelessone, D. and Mencarelli, A. (2011) 'Lattice Discrete Particle Model (LDPM) for failure behavior of concrete. I: Theory', *Cement and Concrete Composites*, 33(9), pp. 881–890. doi: https://doi.org/10.1016/j.cemconcomp.2011.02.011.

Davies, R. and Jefferson, A. (2017) 'Micromechanical modelling of self-healing cementitious materials', *International Journal of Solids and Structures*. Elsevier Ltd, 113–114, pp. 180–191. doi: 10.1016/j.ijsolstr.2017.02.008.

Davies, R., Jefferson, T. and Gardner, D. (2021) 'Development and Testing of Vascular Networks for Self-Healing Cementitious Materials', *Journal of Materials in Civil Engineering*. American Society of Civil Engineers, 33(7), p. 4021164. doi: 10.1061/(ASCE)MT.1943-5533.0003802.

Esgandani, G. A. and El-Zein, A. (2020) 'Thermodynamic based model for coupled elastoplastic damage-healing behaviour of unsaturated geomaterials', *Mechanics of Materials*, 145, p. 103395. doi: https://doi.org/10.1016/j.mechmat.2020.103395.

Ferrara, L., Krelani, V. and Carsana, M. (2014) 'A "fracture testing" based approach to assess crack healing of concrete with and without crystalline admixtures', *Construction and Building Materials*. Elsevier Ltd, 68, pp. 535–551. doi: 10.1016/j.conbuildmat.2014.07.008.

Freeman, B. L. *et al.* (2020) 'A specialised finite element for simulating self-healing quasi-brittle materials', *Advanced Modeling and Simulation in Engineering Sciences*. Springer International Publishing, 7(1). doi: 10.1186/s40323-020-00171-4.

Freeman, B. L. (2022) 'A multi-point constraint unfitted finite element method', *Advanced Modeling and Simulation in Engineering Sciences*. Accepted for publication.

Freeman, B. L. and Jefferson, T. (2020) 'The simulation of transport processes in cementitious materials with embedded healing systems', *International Journal for Numerical and Analytical Methods in Geomechanics*, 44(2). doi: 10.1002/nag.3017.

Gilabert, F. A. *et al.* (2017) 'Integral procedure to assess crack filling and mechanical contribution of polymer-based healing agent in encapsulation-based self-healing concrete', *Cement and Concrete Composites*. Elsevier Ltd, 77, pp. 68–80. doi: 10.1016/j.cemconcomp.2016.12.001.

Gilabert, F. A., Garoz, D. and Paepegem, W. Van (2017) 'Macro- and micro-modeling of crack propagation in encapsulation-based self-healing materials: Application of XFEM and cohesive surface techniques', *Materials & Design*, 130, pp. 459–478. doi: https://doi.org/10.1016/j.matdes.2017.05.050.

Groß, S., Reichelt, V. and Reusken, A. (2006) 'A finite element based level set method for two-phase incompressible flows', *Computing and Visualization in Science*, 9(4), pp. 239–257. doi: 10.1007/s00791-006-0024-y.

Han, K. *et al.* (2021) 'Mechanical response analysis of self-healing cementitious composites with microcapsules subjected to tensile loading based on a micromechanical damage-healing model', *Construction and Building Materials*. Elsevier Ltd, 280, p. 122251. doi: 10.1016/j.conbuildmat.2021.122251.

Hansbo, A. and Hansbo, P. (2002) 'An unfitted finite element method, based on Nitsche's method, for elliptic interface problems', *Computer Methods in Applied Mechanics and Engineering*, 191(47–48), pp. 5537–5552. doi: 10.1016/S0045-7825(02)00524-8.

Hilloulin, B. *et al.* (2016) 'Mechanical regains due to self-healing in cementitious materials: Experimental measurements and micro-mechanical model', *Cement and Concrete Research*, 80, pp. 21–32. doi: https://doi.org/10.1016/j.cemconres.2015.11.005.

Jefferson, A. D. and Freeman, B. L. (2022) 'A crack-opening-dependent numerical model for self-healing cementitious materials', *International Journal of Solids and Structures*, 244–245, p. 111601. doi: https://doi.org/10.1016/j.ijsolstr.2022.111601.

Jefferson, T. *et al.* (2018) 'Research Progress on Numerical Models for Self-Healing Cementitious Materials', *Advanced Materials Interfaces*, 5(17). doi: 10.1002/admi.201701378.

Jiang, T.-S., Soo-Gun, O. H. and Slattery, J. C. (1979) 'Correlation for dynamic contact angle', *Journal of Colloid and Interface Science*, 69(1), pp. 74–77. doi: https://doi.org/10.1016/0021-9797(79)90081-X.

Koenders, E. A. B. (2012) 'Modelling the self healing potential of dissoluble encapsulated cement systems', in.

Lemaitre, J. and Desmorat, R. (2005) *Engineering Damage Mechanics*. Springer.

Li, M., Wittek, A. and Miller, K. (2014) 'Efficient inverse isoparametric mapping algorithm for whole-body computed tomography registration using deformations predicted by nonlinear finite element modeling', *Journal of Biomechanical Engineering*, 136(8). doi: 10.1115/1.4027667.

Di Luzio, G., Ferrara, L. and Krelani, V. (2018) 'Numerical modeling of mechanical regain due to self-healing in cement based composites', *Cement and Concrete Composites*. Elsevier Ltd, 86, pp. 190–205. doi: 10.1016/j.cemconcomp.2017.11.006.

De Nardi, C., Gardner, D. and Jefferson, A. D. (2020) 'Development of 3D Printed Networks in Self-Healing Concrete', *Materials*. Multidisciplinary Digital Publishing Institute, 13(6), p. 1328. doi: 10.3390/ma13061328.

Pande, S., Papadopoulos, P. and Babuška, I. (2021) 'A cut-cell finite element method for Poisson's equation on arbitrary planar domains', *Computer Methods in Applied Mechanics and Engineering*. Elsevier B.V., 383, p. 113875. doi: 10.1016/j.cma.2021.113875.

Rodríguez, C. R. *et al.* (2019) 'Numerical investigation of crack self-sealing in cement-based composites with superabsorbent polymers', *Cement and Concrete Composites*, 104, p. 103395. doi: https://doi.org/10.1016/j.cemconcomp.2019.103395.

Tsangouri, E. *et al.* (2019) 'Feasibility study on real-scale, self-healing concrete slab by developing a smart capsules network and assessed by a plethora of advanced monitoring techniques', *Construction and Building Materials*, 228, p. 116780. doi: https://doi.org/10.1016/j.conbuildmat.2019.116780.

Voyiadjis, G. Z., Shojaei, A. and Li, G. (2011) 'A thermodynamic consistent damage and healing model for self healing materials', *International Journal of Plasticity*, 27(7), pp. 1025–1044. doi: 10.1016/j.ijplas.2010.11.002.

Xin, A. *et al.* (2020) 'Mechanics of bacteria-assisted extrinsic healing', *Journal of the Mechanics and Physics of Solids*. Elsevier Ltd, 139, p. 103938. doi: 10.1016/j.jmps.2020.103938.

Zhang, Y. and Zhuang, X. (2018) 'A softening-healing law for self-healing quasi-brittle materials: Analyzing with strong discontinuity embedded approach', *Engineering Fracture Mechanics*. Elsevier Ltd, 192, pp. 290–306. doi: 10.1016/j.engfracmech.2017.12.018.

Zhou, S. *et al.* (2017) 'Modeling microcapsule-enabled self-healing cementitious composite materials using discrete element method', *International Journal of Damage Mechanics*, 26(2), pp. 340–357. doi: 10.1177/1056789516688835.